FINITE ELEMENT SIMULATION OF THE THERMOELASTIC BEHAVIOUR OF A FUEL ROD

A. SOBA, A. DENIS
Depto. Combustibles Nucleares,
Comisión Nacional de Energía Atómica,
Buenos Aires, Argentina

Abstract

In 1986 the irradiation of the first prototypes of MOX fuels fabricated in Argentina started. The experiment's description, the results of the PIEs and the comparison with the output of the BACO code were published in 1996. In particular, Eddy current testings were performed before and after irradiation. The latter yielded wavelike signals whose amplitude variations can be easily correlated with the pellet distribution through the fuel rod and with the power profile. The present work attempts to give a thermomechanical interpretation of this experimental fact. The pellet and the cladding are simulated by a finite element scheme. Although the results are still preliminary, the tendency of the system to expand preferentially in the vicinity of the pellet's edge is well represented and the results correlate properly with the experimental observations.

1. INTRODUCTION

The first Argentine prototypes of Pressurized Heavy Water Reactor (PHWR) UO_2 (MOX) fuel rods were fabricated and controlled in the α-Facility of the U.A.Combustibles Nucleares of the Comisión Nacional de Energía Atómica (CNEA). The irradiation experiments were carried out in the High Flux Reactor (HFR) of Petten, The Netherlands. The preirradiation destructive examinations of one of the rods and the postirradiation examinations of the others were performed in the Kernforschungszentrum (KfK), Karlsruhe, Germany. Two of the rods included Iodine doped pellets, one of them with elemental Iodine and the other one with CsI, to simulate a starting burnup of about 14-15 GWd/ton(M). Two other non-doped rods were irradiated together for a long period at an average linear power of 230 W/cm to a final burnup of 15 GWd/ton(M). After that, one of them was submitted to a power ramp until an increase of activity in the coolant water was detected, indicating that a failure in the rod had occurred. The detailed description of this experiment is given elsewhere [1].

All the rods were examined after irradiation. Besides the visual inspections, dimensional determinations were performed in both non-doped rods after the base irradiation and in one them also after the power ramp. To this end, Eddy current testings and absolute diameter measurements were carried out. The linear power profiles are shown in Fig. 1. The dimensional results are shown in Figs. 2 and 3, that correspond to the rods labeled A.1.2 and A.1.3 respectively in Ref. [1].

The dimensional characteristics of the fuel rods are:

Pellet height	1.12±0.01 cm
Pellet radius	1.040±0.001 cm
Pellets number	21
Enrichment	1.25%
Cladding inner radius	0.5225 cm
Cladding outer radius	0.5825 cm
Gap thickness	0.0025 cm

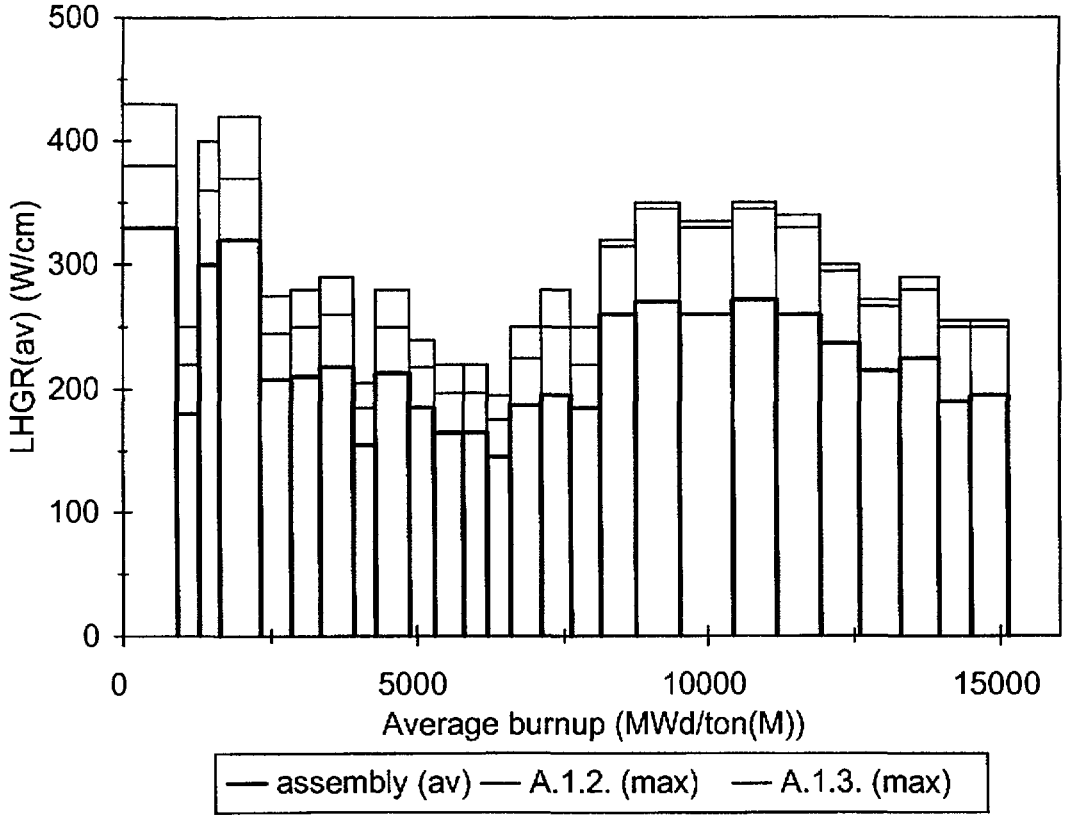

FIG. 1.a. Linear heat generation rate during stationary irradiation of rods A.1.2 and A.1.3.

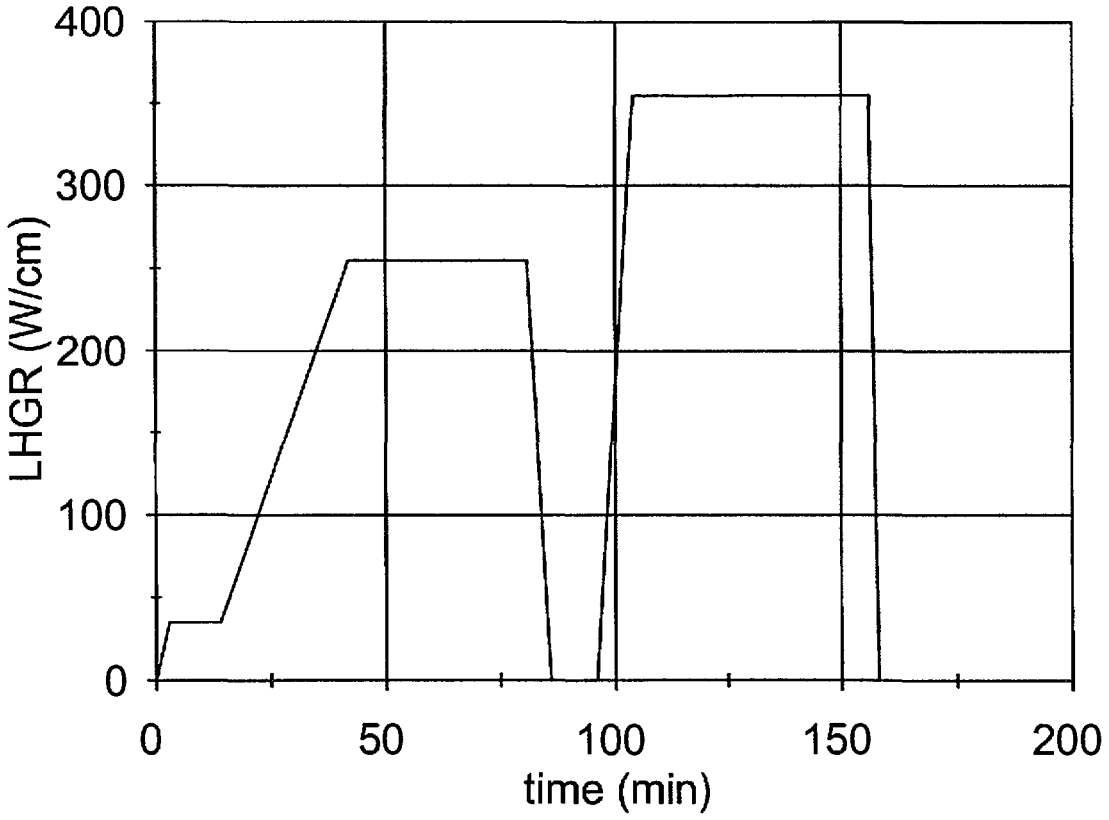

FIG. 1. b. Linear power ramp applied to rod A.1.3 after the stationary irradiation of a.

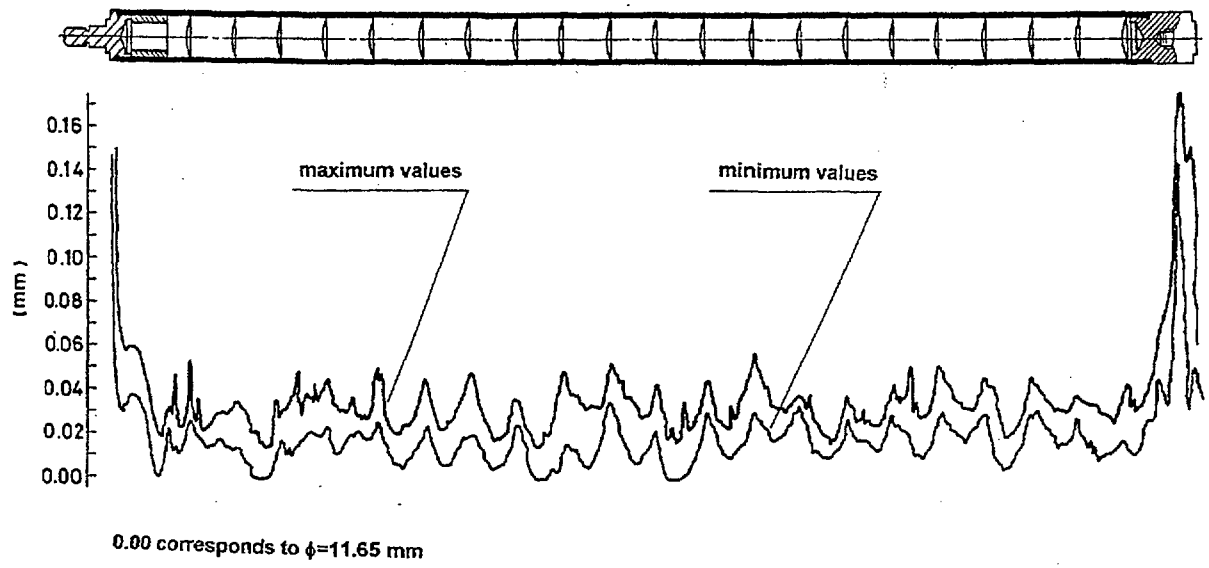

FIG. 2. Dimensional profile of rod A.1.2 after stationary irradiation.

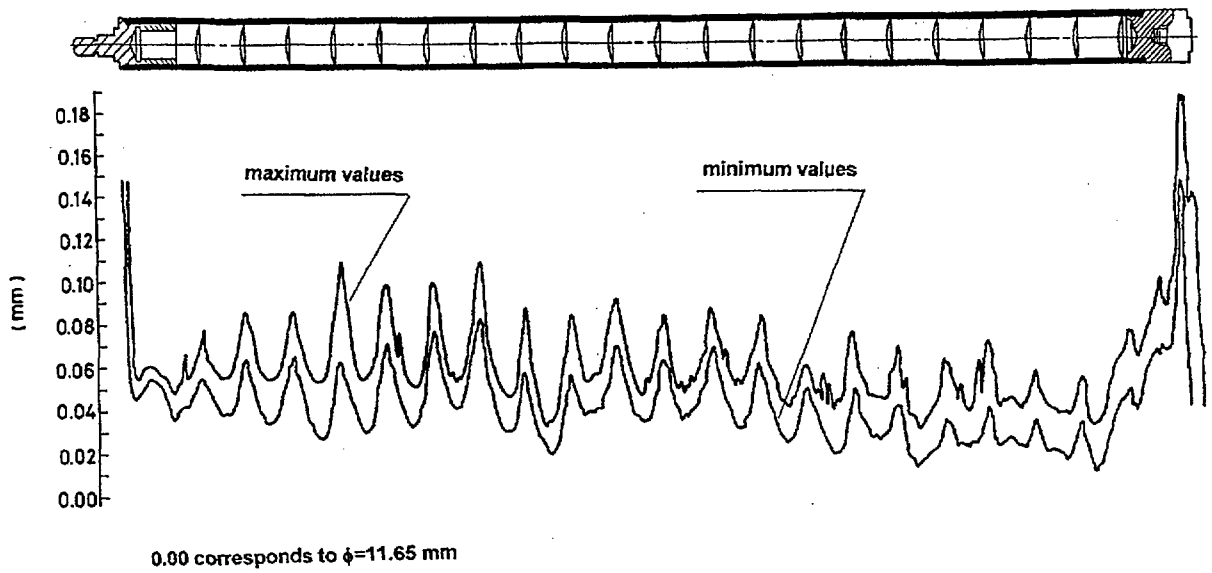

FIG. 3. Dimensional profile of rod A.1.3 after stationary irradiation and power ramp.

2. PROPOSED MODEL

The pellet, the cladding and the gap between them are simulated by the finite element method. A scheme of the system representing a longitudinal section of the fuel rod is shown in Fig. 4.

Due to the high temperatures developed within the pellet, particularly at its center line, and to the strong temperature gradient that consequently appears, the cylindrical pellet surface distorts: it bends outwards, the top and bottom faces being displaced further than the central belt [2]. The dimensional changes in the fuel rod provoked by thermal expansion may induce pellet-cladding interaction (PCI) and the consequent plastic cladding strain [3].

To simulate this problem the thermal and elastic coupled equations have to be solved.

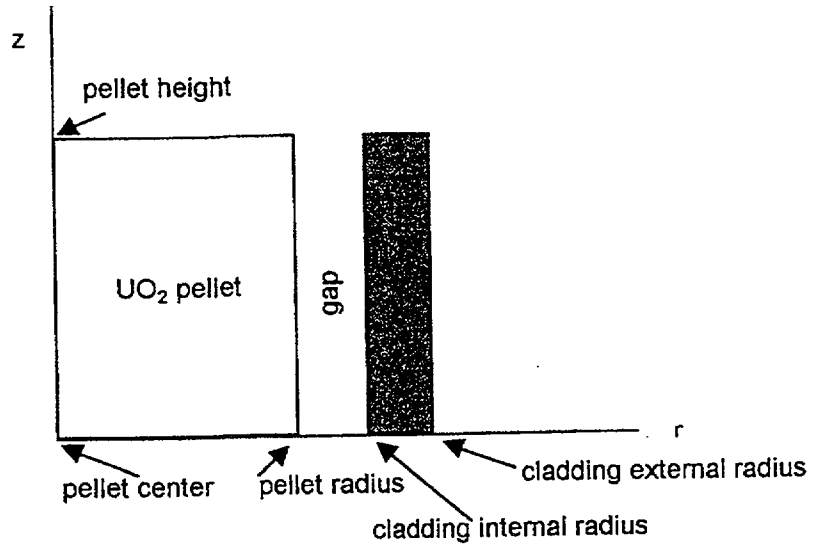

FIG. 4. Scheme of the longitudinal section of the pellet-gap-cladding system.

2.1. The thermal problem

Since the system has axial symmetry, cylindrical coordinates are employed. The temperature depends on r and z only. If T represents the temperature, Q is the volumetric heat generation rate, $\kappa=\kappa(T)$ is the thermal conductivity and assuming steady-state heat transfer conditions, the temperature distribution in each material is obtained by solving the differential equation:

$$\kappa\left(\frac{1}{r}\frac{\partial}{\partial r}\left(r\frac{\partial T}{\partial r}\right)+\frac{\partial^2 T}{\partial z}\right)+Q=0$$

with the boundary conditions: T=300°C at the cladding external radius (Dirichlet condition) and ∇T=0 (Neumann condition) at the remaining portion of the system boundary.

Application of the finite element method involves definition of a mesh, which in this case is chosen of triangular elements, definition of the corresponding shape functions, approximation of the continuous unknown function T by a linear combination of the shape functions. A system of linear equations is finally obtained, one equation for each unknown nodal value. The matrix formulation of the problem is:

$$[k^e]\{\Phi^e\}=\{f_Q^e\}-\{I^e\} \qquad \text{(A)}$$

where the superscript e indicate a magnitude referred to an element, $[k^e]$ is the element stiffness matrix defined as

$$[k^e]=2\pi\bar{r}A[B]^T[D][B], \qquad \text{(B)}$$

$\bar{r}$ is the radial distance to the centroid of the element, A is the element area, the coefficients in the matrix B are obtained differentiating the shape functions relative to r and z,

$$D=\kappa\begin{bmatrix}1 & 0\\ 0 & 1\end{bmatrix},$$

the column vector $\{\Phi^e\}$ contains the nodal values of the unknown function,

$$\{f_Q^e\}=\int_V Q[N]^T dV,$$

the row vector $[N]$ contains the shape functions and the column vector $\{I^e\}$ contains the Neumann boundary conditions, which in the present case are zero.

The solution of the heat transfer problem becomes the input to the stress analysis problem and the same discretization is used to solve both.

2.2. The constitutive equations

Given the axial symmetry of the system, neither the geometry nor the surface loading depends on the angular coordinate. The displacements, strains and stresses are functions of r and z only. Let us represent with u and w the displacements in the r and z direction, respectively. The strain-displacement relations are [4]:

$$e_{rr} = \frac{\partial u}{\partial r} \;;\; e_{\theta\theta} = \frac{u}{r} \;;\; e_{zz} = \frac{\partial w}{\partial z} \;;\; e_{rz} = \frac{\partial u}{\partial z} + \frac{\partial w}{\partial r} \;;\; e_{r\theta} = 0 \;;\; e_{z\theta} = 0$$

The four non-zero components of the strain are placed in the column vector $\{e\}$:

$$\{e\}^T = [e_{rr} \quad e_{\theta\theta} \quad e_{zz} \quad e_{rz}]$$

The strain components are separated into elastic ($\{\varepsilon\}$) and thermal ($\{\varepsilon_{th}\}$) strains:

$$\{e\} = \{\varepsilon\} + \{\varepsilon_{th}\}$$

where:

$\{\varepsilon\}^T = [\varepsilon_{rr} \quad \varepsilon_{\theta\theta} \quad \varepsilon_{zz} \quad \varepsilon_{rz}]$ and $\{\varepsilon_{th}\}^T = [\alpha\Delta T \quad \alpha\Delta T \quad \alpha\Delta T \quad 0]$

and α is the thermal expansion constant.

According to the elasticity theory, for small deformations, the stresses depend linearly on deformations. This is the Hooke's law which in matrix form is expressed as:

$$\{\sigma\} = [D]\{\varepsilon\}$$

where the vector of stress components is

$\{\sigma\}^T = [\sigma_{rr} \quad \sigma_{\theta\theta} \quad \sigma_{zz} \quad \sigma_{rz}]$

and $[D]$ is the material matrix given by:

$$[D] = \frac{E}{1+\mu}\begin{bmatrix} d & b & b & 0 \\ b & d & b & 0 \\ b & b & d & 0 \\ 0 & 0 & 0 & 1/2 \end{bmatrix} \quad \text{with} \quad d = \frac{1-\mu}{1-2\mu} \quad \text{and} \quad b = \frac{\mu}{1-2\mu}$$

The constants E and μ are the Young's modulus and the Poisson's ratio, respectively.

When the finite element method is applied, the unknown displacements u and w are written in terms of the element nodal values and the shape functions. The above differential equations are thus transformed to linear equations:

$$\begin{Bmatrix} u(r,z) \\ w(r,z) \end{Bmatrix} = [N]\{U^e\}$$

The strain-displacement relationships yield:

$$\{e\} = [B]\{U^e\}$$

The matrix formulation of the problem is:

$$[k^e]\{U^e\} = \{f^e\} - \{I^e\}$$

which is formally identical to that employed for the thermal problem (1) , the matrix $[k^e]$ is defined as in (2) with the corresponding expressions for matrices $[B]$ and $[D]$. The term $\{f^e\}$ contains the contributions of the thermal force and of the external pressure:

$$\{f^e\} = \int_V [B]^T [D]\{\varepsilon_{th}\} dV + \int_\Gamma [N]^T \begin{Bmatrix} p_r \\ p_\theta \\ p_z \end{Bmatrix} d\Gamma$$

where Γ is the external element surface of volume V. The term $\{I^e\}$ contains the Neumann boundary conditions, which are zero as in the thermal problem [4].

The physical constants employed in the present calculations are listed in Table I.

TABLE I.

Young's modulus E (N cm^{-2})		
	UO_2:	$2.065\text{x}10^7\ (1+1.091\text{x}10^{-4}\ T)$ [5]
	Zry:	$1.236\text{x}10^7\text{-}6.221\text{x}10^3\ T$ [5]
Poisson's ratio μ		
	UO_2:	0.316 [5]
	Zry:	0.32 [5]
Thermal expansion α (K^{-1})		
	UO_2:	$(-4.972\text{x}10^{-4} + 7.107\text{x}10^{-6}\ T + 2.583\text{x}10^{-9}\ T^2)/\Delta T$ [5]
	Zry:	$(-2.07\text{x}10^{-3} + 6.72\text{x}10^{-6}\ T)/\Delta T$ [5]
Thermal conductivity κ (W cm^{-1}K^{-1})		
	UO_2:	$\left[\frac{40.4}{464+T} + 1.216\text{x}10^{-4} \exp(1.867\text{x}10^{-3}\ T)\right]$ [5]
	Zry:	$7.51\text{x}10^{-2} + 2.09\text{x}10^{-4}\ T - 1.45\text{x}10^{-7}\ T^2 + 7.67\text{x}10^{-11}\ T^3$ [5]
	He:	$3.366\text{x}10^{-3}\ T^{0.668}$ [5]
temperatures T in K.		

3. CALCULATION PROCEDURE

3.1. The numerical method

The domain discretization in performed by means of linear triangular elements. The mesh employed in the calculations contains 179 nodes and 311 elements divided into three groups, corresponding to each material of the system: UO_2 pellet, gaseous gap and Zry cladding. A non uniform mesh is chosen in order to have a more detailed description in the region where the greater variations are expected. To this end, an element side length of 0.2 cm is chosen at the pellet center and of 0.05 cm at the pellet outer radius, in the gap and in the cladding wall. The discretization was carried out with the bidimensional mesh generator DELAUNAY 2.0 developed at CAB-CNEA; the result is shown in Fig. 5.

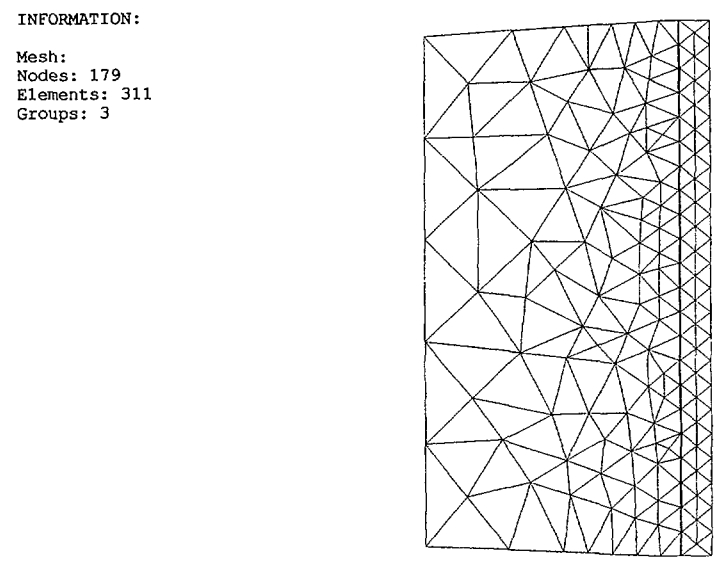

FIG. 5. Finite element discretization of the system.

3.2. The calculation program

The calculation program was written in FORTRAN and consists of approximately 1300 statements. The graphical inputs and outputs were developed in C.

The power history and the boundary conditions constitute the data entry. The code solves the heat transfer equation by the finite element method and gives the temperature distribution in the 3-phases system in each step. Then, the elasticity equations are solved, where the term $\alpha \Delta T$ contains the temperature variation between two consecutive steps. The elastic problem is also solved by the finite element method, the displacements U in each node and in each direction (r and z) are determined, the new coordinates of the nodes are evaluated and the calculation procedure restarts. The stress and strain state at each element are also obtained in each power step.

The output of the thermal problem is visualized by means of the program CONTOURS elaborated at CAB-CNEA while that of the elastic problem is obtained with MATLAB.

The equations systems are solved by the diagonalization method of Gauss. The calculation time required is of about 10 s per step, for the mesh dimensions employed in the present work and using an equipment PC of 32Mb RAM with a Pentium processor of 200 MHz. The power histories involved contain 27 steps of nearly constant power (rod A.1.2) or 90 steps when a final power ramp is included (rod A.1.3).

4. RESULTS AND DISCUSSION

The temperature distribution within the system before deformation is represented in Fig. 6. The isothermal lines run parallel to the axial direction; slight departures due to the discretization process are observed near the pellet center, where the element's size is larger.

Thermal expansion induces dimensional changes in the radial direction, particularly in the pellet. This expansion is more pronounced near the pellet's edges. A magnification of the outer region of the rod is seen in Fig. 7 where the curved shape of the cladding and the pellet is evident. The plot was obtained by simulating the power history of rod A.1.3 (stationary irradiation followed by final power ramp). Although only the elastic behaviour is considered in the model, a permanent deformation is achieved.

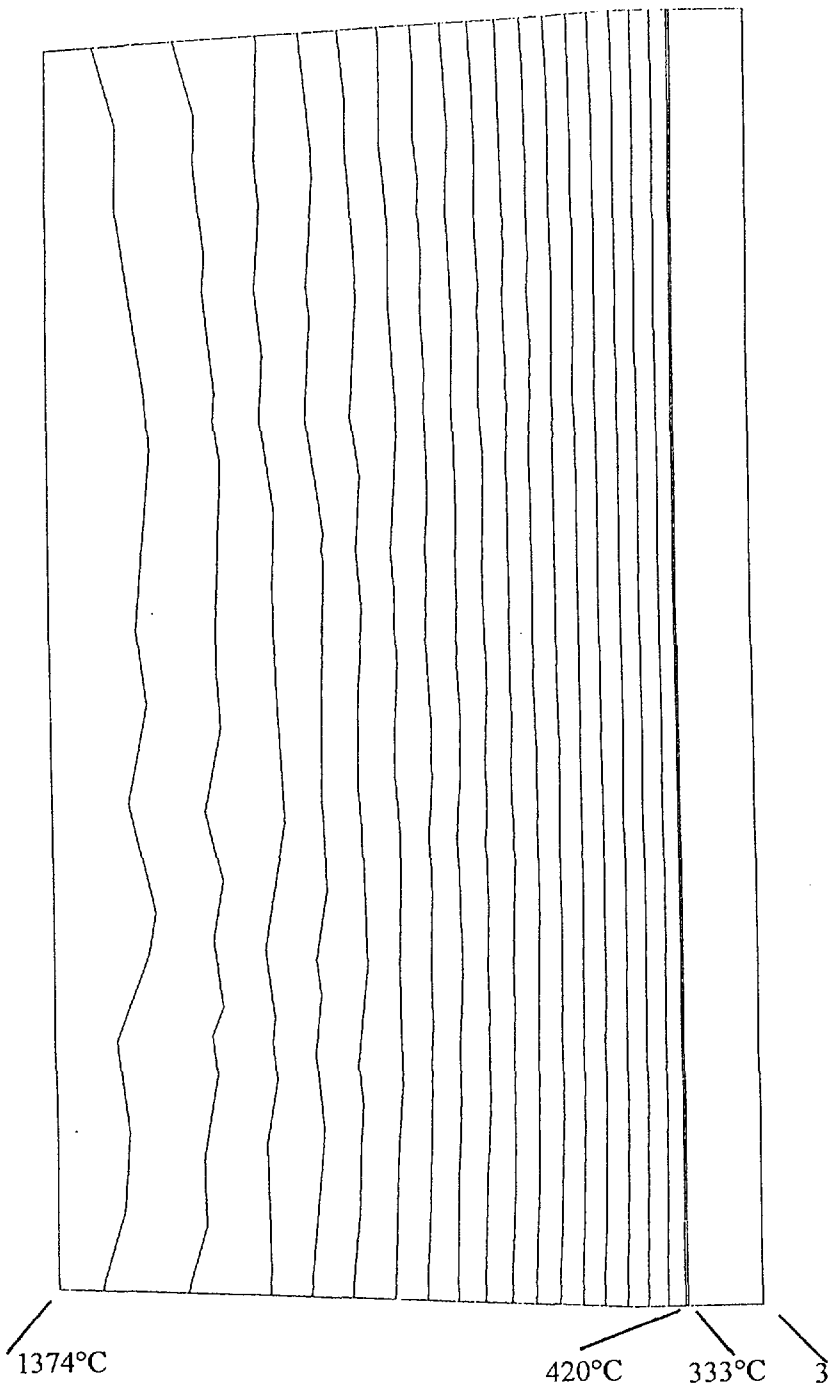

FIG. 6. Temperature distribution in the undeformed system under a linear power of 380W/cm.

This feature becomes clear from Fig. 8 where the evolution of the pellet outer and the cladding inner radii are compared. The apparent inversion between both indicates that the code predicts solid pellet-cladding contact. When this condition appears, a contact pressure between both materials is applied, which effect is to push the cladding outwards.

In Figures 9 and 10 the magnification of the outer cladding boundary after irradiation is shown. The former corresponds to the calculation results obtained with the maximum power and the latter, with the average power. The results obtained after stationary irradiation (rod A.1.2) and after stationary irradiation followed by power ramp (rod A.1.3) are superimposed for comparison. The more remarkable feature is the presence of ridges on the external surface of the cladding accompanying the pellets' distribution. Both rods have experienced a general radius increase, as can

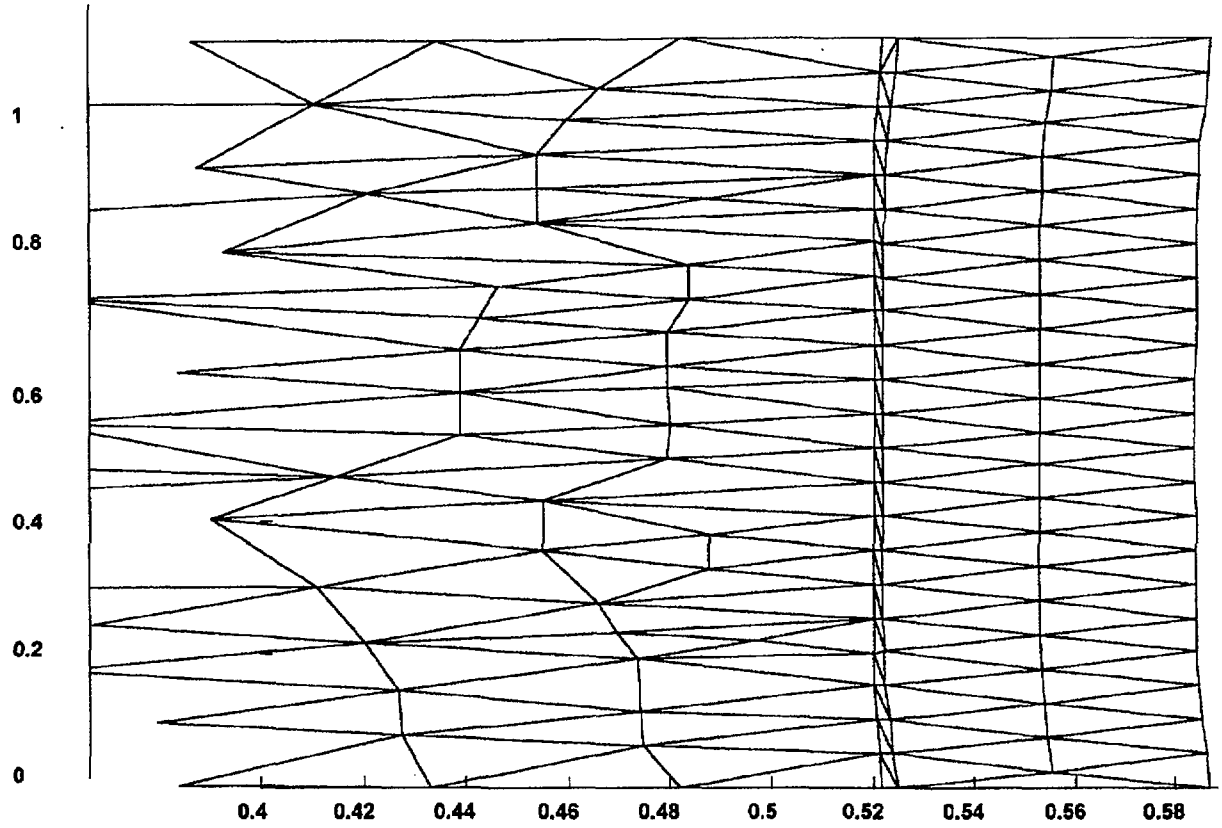

FIG. 7. Effect of irradiation with average power on the pellet and cladding shape of rod A.1.3 after power ramp.

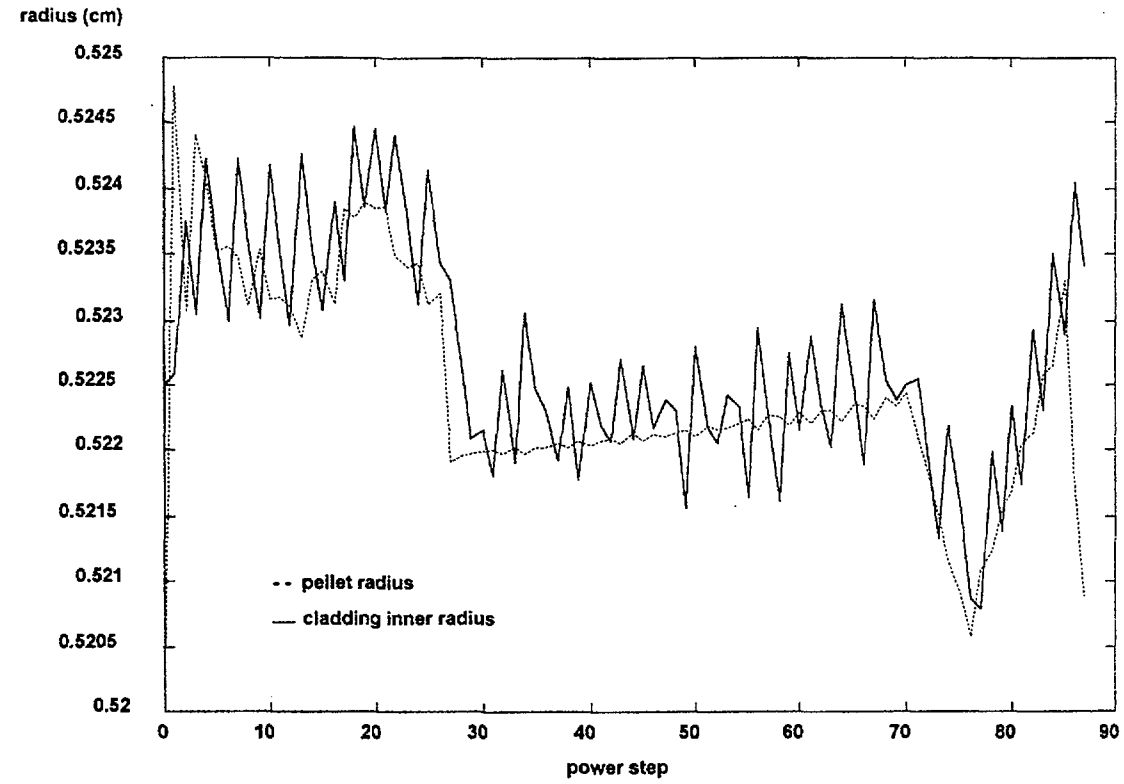

FIG. 8. Evolution of the radius in the belt region of rod A.1.3 during irradiation with maximum power followed by power ramp.

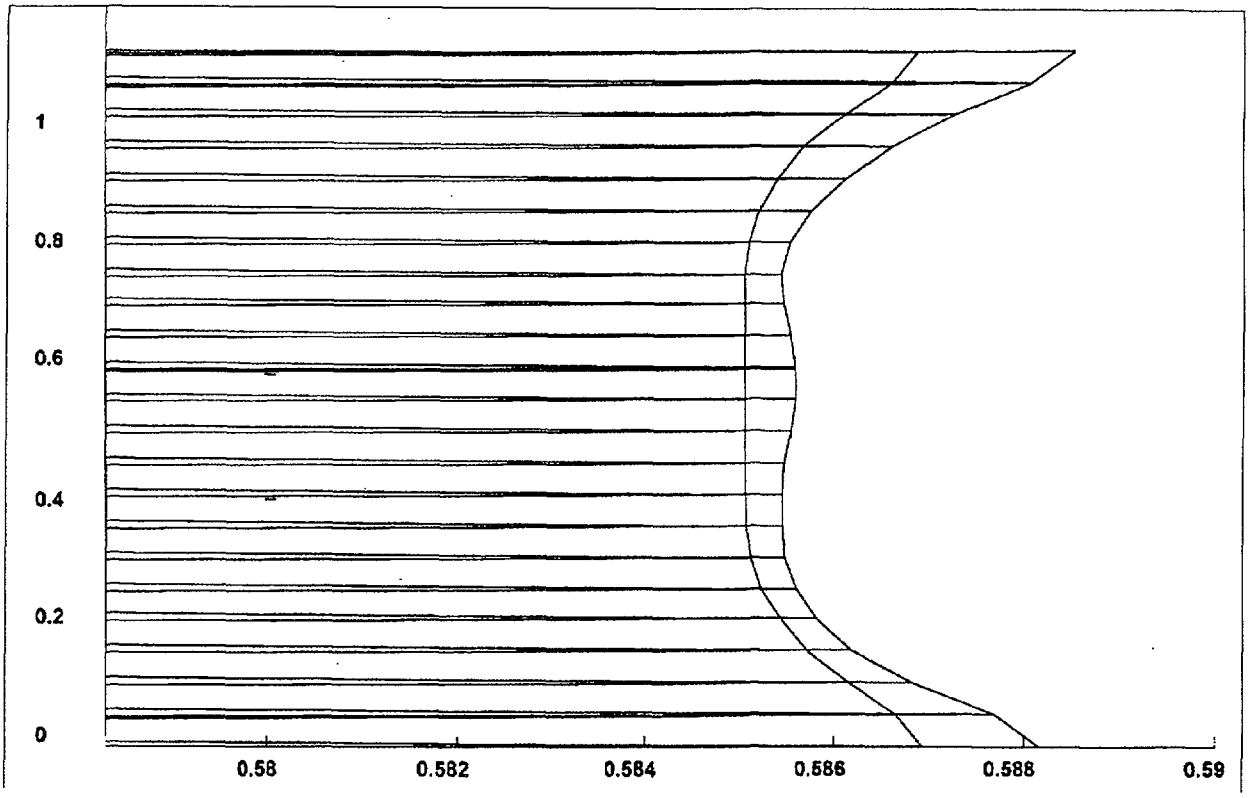

FIG. 9. Comparison between the external boundary final shapes of rods A.1.2 and A.1.3 with maximum power.

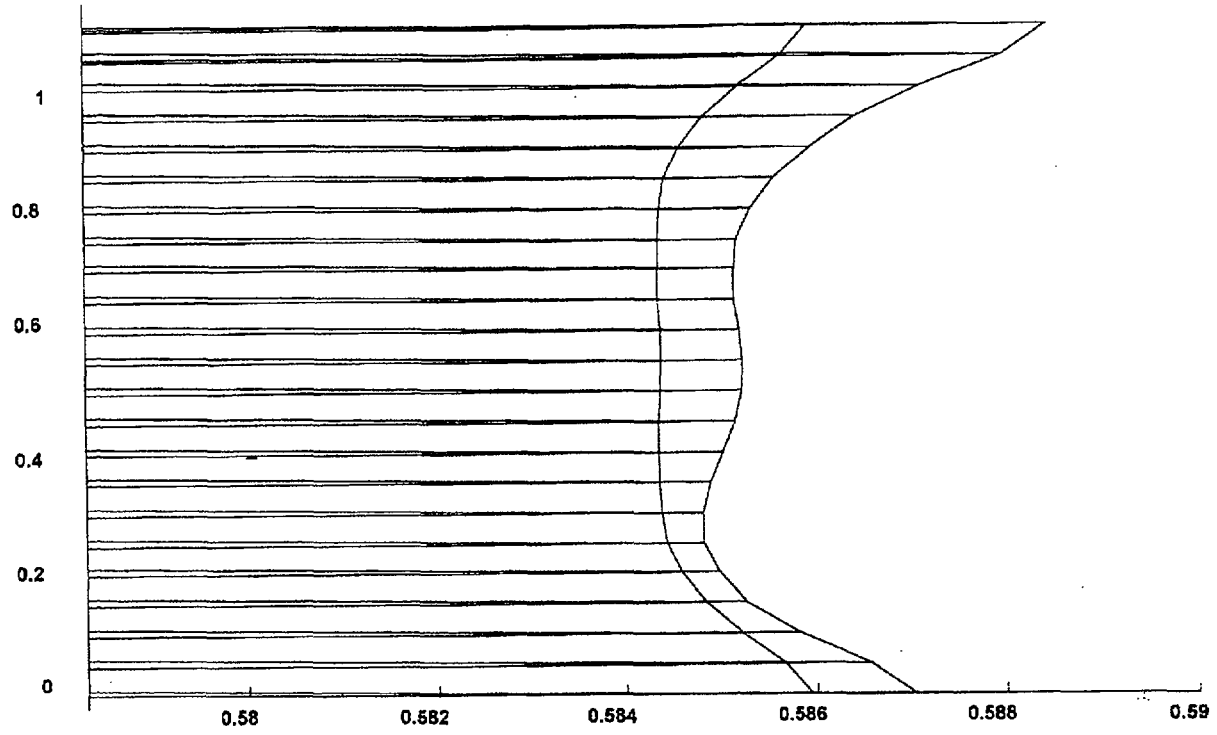

FIG. 10. Comparison between the external boundary final shapes of rods A.1.2 and A.1.3 with average power.

be seen by comparing the clad belt radii with the initial radius of 0.5825 cm. It is visible that the power ramp has a strong effect on the cladding permanent deformation, which is of 0.3% for the rod A.1.2 and 0.55% for the rod A.1.3. This effect is more significant on the crests, where the deformation is of about 0.6% and 1%, respectively.

The experimental results shown in Figures 2 and 3 reveal that for rod A.1.2 the crests' height ranges between 18 and 30 μm and for rod A.1.3, between 28 and 55 μm. The calculations performed in the present work predict values in the ranges 16 to 18 μm in the first case and 29 to 33 μm in the second, the band being due to using the average or the maximum power as input.

5. CONCLUSIONS

The thermoelastic code developed in this work is able to reproduce with reasonable accuracy the deformation of a fuel rod that has undergone either a stationary power history or a power ramp. The results agree with those obtained with the BACO code [1].

As the results presented in the previous section reveal, the calculated figures fall within the lower end of the experimental results range. Given that the model only contains the elastic effects, this seems to indicate that incorporation of the inelastic effects, which will be the next step in the work, will improve the results. The phenomena of creep and swelling will be also incorporated in the near future.

ACKNOWLEDGEMENTS

The authors wish to thank Lic. Pablo Adelfang for his continuous interest on this work and for the contribution of the experimental data.

REFERENCES

[1] MARINO, A.C., PÉREZ, E.E., ADELFANG, P., Journal of Nuclear Materials 229 (1996) 169-186.

[2] MATHEWS, J.R., The quantitative description of deformation and stress in cylindrical fast reactor fuel pins, in Advances in Nuclear Science and Technology, Vol.6 (1972), Academic Press.

[3] CAILLOT, L., LINET, B., LEMAIGNAN, C., Pellet clad interaction in PWR fuel. Analytical irradiation experiment and finite element modelling, (Proc. SMIRT 12, Stuttgart, Germany, 1993).

[4] SEGERLIND, L.J., Applied finite element analysis, 2nd Ed., Wiley (1984).

[5] Handbook of materials properties for use in the analysis of light water reastor fuel behaviour, MATPRO version 11, NUREG/CR-0497, TREE-1280 (1979).